High pressure strengthening in ultra-fine-grained metals

X.L. Zhou[1, 2, 3+], Z.Q. Feng[4+], L.L. Zhu[5+], J.N. Xu[1,6+], L. Miyagi[3], H.L. Dong[1], H.W. Sheng[1], Y.J. Wang[1], Q. Li[7,8], Y. M. Ma[7,8], H.Z. Zhang[1], J.Y. Yan[2], N. Tamura[2], M. Kunz[2], K. Lutker[9], T.L. Huang[10], D.A. Hughes[11], X. Huang[4]* and Bin Chen[1]*

[1]Center for High Pressure Science and Technology Advanced Research, Pudong, Shanghai 201203, China

[2]Advanced Light Source, Lawrence Berkeley National Lab, Berkeley, CA 94720, USA

[3]Department of Geology and Geophysics, University of Utah, Salt Lake City, UT 84112, USA

[4]International Joint Laboratory for Light Alloys (MOE), College of Materials Science and Engineering, Chongqing University, Chongqing 400044, China

[5]Center for X-Mechanics & Key Laboratory of Soft Machines and Smart Devices of Zhejiang Province, School of Aeronautics and Astronautics, Zhejiang University, Hangzhou 310027, China

[6]Department of Physics, Fudan University, Shanghai 200438, China

[7]State Key Lab of Superhard Materials & Innovation Center for Computational Physics Methods and Softwares, College of Physics, Jilin University, 130012, Changchun, China

[8]International Center for Future Science, Jilin University, 130012, Changchun, China

[9]Department of Chemistry, University of California, Berkeley, CA 94720, USA

[10]Shenyang National Laboratory for Materials Science, Chongqing University, Chongqing 400044, China

[11]Fremont, CA, USA

+These authors contribute equally to this project.

*Corresponding authors. Email: chenbin@hpstar.ac.cn, xiaoxuhuang@cqu.edu.cn

The strengthening of polycrystalline metals based on grain refinement has previously been reported to be no longer effective below a critical grain size of approximately 10-15 nm (Refs. 1, 2). That report imposed a limit on grain size tuning for synthesizing stronger materials. Here, we report our study using a diamond-anvil cell coupled with radial X-ray diffraction to track *in situ* the yield stress and deformation texturing of pure nickel samples with various average grain sizes. Continuous strengthening is observed from 200 nm to the minimum grain size of 3 nm. Strengthening as a function of grain size is enhanced in the lower grain size regime below 20 nm. We achieved an ultra-high strength of ~ 4.2 gigapascals in nickel, 10 times larger than the values for commercial nickel material. The maximum flow stress of 10.2 gigapascals is reached in 3 nm nickel in the pressure range of this study. Plasticity simulation and transmission electron microscopy (TEM) examination reveal that the high strength observed in 3 nm nickel is caused by the superposition of strengthening mechanisms: partial and full dislocation hardening plus grain boundary plasticity suppression. These results rejuvenate the search for ultra-strong metals via materials engineering.

Understanding the strengthening of nanograined metals has been puzzling, as both mixed results of size softening and hardening have been reported[3-6]. The main challenges in resolving this debate are the difficulty in synthesizing high quality, ultrafine metal samples for traditional tension or hardness tests and making statistically reproducible measurements. Some researchers have pointed out that reported size softening may be related to materials preparation[7]. Porosity, amorphous regions and impurities may be introduced during sample preparation methods like inert gas condensation and electrodeposition, leading to softening in micro-hardness measurements and tension tests. Another difficulty is the ambiguity in identifying the dominant plastic deformation mechanisms of nanograined metals. Various defects or processes at the nanoscale have been reported, including dislocations[8,9], deformation twinning[10,11], stacking faults (SFs)[10], GB migration[12], GB sliding[1], and grain rotation[13,14]. Hence the processes that dominate plastic deformation and thus determine the strength of nanograined metals are still unclear. In this study, we employ radial diamond-anvil cell (rDAC) X-ray diffraction (XRD) techniques to track *in situ* the yield stress and deformation texturing of nickel of various grain sizes. We find that mechanical strengthening can be extended down to a grain size of 3 nm, much smaller than the previously reported strongest sizes of nanograined metals. This finding pushes mechanical strengthening to the lowest record grain size, demonstrating the potential for achieving ultrahigh strengths in metals.

Radial DAC XRD experiments (Extended Data Fig. 1, see Supplementary Information) were performed at beamline 12.2.2, Advanced Light Source (ALS), Lawrence Berkeley National Laboratory and Shanghai Synchrotron Radiation Facility (SSRF). Eight nickel samples made from particle (grain) sizes ranging from 3 to 200 nm (Extended Data Figs. 2-3) were measured. The relatively narrow size distributions allow for the investigation of the size dependence of the material's strength. In the sample under uniaxial compression, the stress can be separated into hydrostatic and differential stress components. The differential stress between the maximum and minimum compression directions can be obtained according to lattice strain theory[15] (see Supplementary Information). The measured XRD peak positions provide information on differential strains as well as differential stresses (Fig. 1a). Plastic deformation has an influence on lattice strains measured using diffraction, and so the differential strain/stress measured with radial DAC XRD can capture the transition from elastic to plastic deformation dominant behaviors and provide the information of yield strength, strain hardening, etc (Fig. 1 and Extended Data Fig. 4). At the same pressure, the differential strain of the 3 nm-sized nickel is higher than that of larger grained counterparts. The larger curvatures (ellipticity of the XRD rings which translates into non-linearity of the lines plotted along the azimuth angle) of diffraction lines for smaller nanocrystals indicate higher elastic deformation and greater ability for the material to support differential stress in the crystal plane without plastic deformation. The Rietveld refinement implemented in the MAUD software[16] was used to analyze the differential strain and texture of our samples at each pressure. The average differential stress of nickel vs its lattice strain can thus be obtained (Fig. 1b) according to Eqs. (5-9) (see Supplementary Information). To remove the effect of hardening induced by hydrostatic pressure, we performed Elasto–ViscoPlastic Self-Consistent (EVPSC)[17] simulations (see Supplementary Information) to simulate the stress-strain curves of nickel at ambient conditions (Extended Data Fig. 5). This enables the comparison of our extrapolated strength results at zero pressure with those of conventional tests [2,18] (Fig. 1c). The stress-strain curves (Fig. 1b and Extended Data Fig. 5c) show that instead of softening, smaller grained nickel was stronger than its coarser counterparts, in a strong contrast to the results of previous studies (Fig. 1c). Stress-strain curves of finer nano nickel also show a larger slope/hardening exponent (Fig. 1b), possibly due to the increased plastic anisotropy in this smaller grain size (Extended Data Fig. 5). We note that a slight strength drop of 40 nm nickel in EVPSC simulations and the cause remains to be further investigated.

The development of *in-situ* deformation textures for nanograined nickel with various grain sizes was captured at different strains. As shown in Fig. 2, nickel samples with larger grain sizes above 20 nm show very strong deformation textures even at low strain. Nanograined nickel samples sized below 20 nm exhibit very weak deformation textures, indicating that traditional full dislocation activity become less active, whereas the strength increases with decreasing grain size. Meanwhile, all of the nickel samples develop a deformation texture, indicating that deformation mechanisms may still be based on dislocation slip and twin formation since GB mediated mechanisms would maintain the initial random textures.

Previous simulations[1,19,20] have suggested that GB deformation plays a decisive role in the deformation mechanisms of sub-10-nm-sized nanomaterials. Those studies proposed that size softening would occur due to the transition from dislocation-mediated to GB-mediated mechanisms. In our experiments, however, we observed no size softening but only size strengthening. The uniaxial compressional stress comprises hydrostatic and differential stress components. Although the shear stress arising from the differential stress could potentially activate GB mechanisms, while the hydrostatic stress of the compression increases the critical shear stress for GB migration and sliding, thereby suppressing those mechanisms (Eq. 15). To explore the mechanisms for continuous size strengthening, we simulated the critical stress for activating full and partial dislocations and for activating GB deformation (GB sliding and migration) in nanograined nickel. As shown in Fig. 3a, full dislocations are activated preferentially and are more dominant than partial dislocations above the critical grain size d_c^1. The dislocation-dominant deformation shifts to GB-dominant deformation for grain sizes below a critical value d_c^2. However, compression has a remarkable effect on this shift. The critical stress for activating GB deformation increases with pressure, resulting in the critical grain size d_c^2 being highly pressure-dependent. For example, the critical grain size for active GB deformation of nickel at >1 GPa is <2 nm (Fig. 3b), suggesting that almost no GB deformation is activated in our experiments since hydrostatic pressure is higher than 1 GPa, i.e. the GB-deformation associated softening of fine nano grains has been greatly inhibited during compression. Consequently, when GB-associated deformation (extrinsic deformation) is suppressed, the strength of materials would be determined mainly by intrinsic deformation properties, which are associated with lattice strain and defects in the interiors of grains.

It is known that the critical stress to activate dislocations increases with decreasing grain size. In a simplified analytical dislocation model which considers partial dislocations emitted from GBs of nano grains, the critical stress for emitting a full and partial dislocation[21] can be described as

$$\tau_{\mathrm{f}} = \frac{Gb_f}{d}, \tag{1}$$

$$\tau_p = \frac{Gb_p}{3d} + (1-\delta)\frac{\gamma}{Gb_p}, \tag{2}$$

where b_f and b_p are the Burgers vectors of the full and partial dislocations, respectively; G is the shear modulus; γ is the stacking fault energy; and δ is the ratio of equilibrium stacking fault width to grain size. The critical stresses for nucleating both full and partial dislocations increase sharply as the grain size decreases towards the lower limit (Fig. 3a). This leads to the increase of yield strength at small grain size. Furthermore, partial dislocations are preferentially activated and overtake full dislocations below a critical grain size.

We studied the deformation behavior of nanograined nickel by molecular dynamics (MD) simulations[22] (Fig. 3d). Two types of planar defects associated with partial dislocations, i.e. nanotwins and stacking faults, as well as full dislocations are found in nanograined nickel under compression. To explore the deformation mechanism, we conducted transmission electron microscopy characterization on the recovered samples. As expected, high densities of full dislocation are seen in the coarse-grained sample (Fig. 4d). Remarkably full dislocations are prevalent at all average grain sizes including the finest at 3 nm (Figs. 4a-c), albeit for the 3 nm sample dislocations were observed in grains with slightly larger sizes than average. A detailed analysis of the four dislocations observed in the lower part of Fig. 4a is shown in the sketch in Fig. 4b based on the Thompson tetrahedron. Each of these dislocations is an extended dislocation composed of a stacking fault and two partial dislocations lying on {111} slip planes. It is interesting to note that a Lomer-Cottrell lock and a stair rod are formed from the reactions of partials associated with the upper three dislocations, the latter lies on a {100} plane. These reaction products are immobile and thus provide a strong strengthening effect. A rough estimate of the density of full dislocations based on the dislocations in Fig. 4a suggests a density of $\sim 10^{16}$ m^{-2} that provides a strong strengthening component for the flow stress. At the finest grain sizes nanotwins form bounded by stacking faults, creating important new additions to the deformed structure. These nanotwins further refine the nano structure and contribute to boundary strengthening by constraining dislocation motion. Steps in the twin boundaries are observed forming incoherent twin boundaries that contain partial dislocations (Fig. 4). We note that the simultaneous and cooperative activation of different Shockley partial dislocations on parallel and neighboring glide planes may be responsible for these twins[23]. Stacking faults may expand under high stress, increasing their energy and making it favorable to form low energy twins[24]. Fivefold symmetry twins are also seen in both 3 and 20 nm quenched nickel samples (Fig. 4). Fivefold twins may preexist in the particles or form by the successive emission of partial dislocations from incoherent twin boundaries (ITBs) with high energy. The non-parallel TBs give rise to strong overlapping of associated lattice strain fields, resulting in higher yield strength compared to those without fivefold twinned structures[25]. This result is consistent with our observations in the mechanical measurements (Fig. 1b). In short, twinning and stacking faults observed in our TEM measurements originate from the nucleation and motion of partial dislocations. This provides compelling evidence that in the sub-20 nm regime of grain size, full-dislocation-mediated deformation shifts to both full and partial dislocations combined with deformation twinning.

Our strength measurements (Fig. 1b), computational simulations (Fig. 3a and Fig. 3c) and TEM observations (Fig. 4) indicate that a critical grain size (around 20 nm) exists and corresponds to the shift in deformation mechanisms from full dislocation to full plus partial dislocation mediated deformation. This does not generate a maximum strength at the critical grain size but starts a stronger mode for strengthening. Notably, as shown in Fig. 4, the twins in 20 nm or smaller nickel grains are usually only several nanometers thick, but unlike growth twins, no softening is induced in pressurized nickel nanograins. Instead, size strengthening of nickel is even more pronounced in the smaller size range of nanograins. As shown in Fig. 3c, below 20 nm the measured yield strength of nanograined nickel largely deviates from the trend predicted by the traditional Hall-Petch model. Considering that the contribution of partial dislocations becomes significant in fine nanograins, we propose a modified Hall-Petch relationship as follows:

$$\sigma_y = \sigma_0 + \frac{k_0}{\sqrt{d}} + \frac{k_1}{d} \tag{3}$$

where σ_y and d represent the yield strength and grain size, respectively, and σ_0, k_0 and k_1 are constants. The first two terms represent the friction stress and Hall-Petch formulation associated with full dislocation boundary interaction. The third term is related to the partial dislocation contribution to yielding, which is inversely proportional to grain size d according to Eq. 2. The fitting of our experimental data with Eq. 3 shows that this new model reflects the effects of both full and partial dislocations, can describe the size strengthening of metals in a wide size range. We note that this fit gives a high friction stress of ~1.1 GPa, k_1 of $9\,\mathrm{MPa \cdot \mu m}$ and a low k_0 of 101 MPa/μm$^{-1/2}$ compared to conventionally deformed Ni with 20 MPa and 158 MPa/μm$^{-1/2}$, respectively[26,27]. To check the generality of the size strengthening for nanograined metals, we conducted similar high-pressure deformation experiments on nanograined gold and palladium. A similar enhanced strengthening effect at the lowest grain sizes was observed, which indicates that this full plus partial dislocation-mediated strengthening is common in compressed nanograined metals.

This size strengthening effect may apply not only to high pressure cases but also provide guidance for applications at ambient conditions. A recent study[28] reported that a twofold increase in hardness was achieved in nanograined Ni-Mo alloys by stabilizing GB through Mo segregation. With this technique yield strengths of ~1.6 and 3.8 GPa were achieved in Ni and Ni-Mo alloys, respectively. In our experiments, an ultra-high strength of ~4.2 GPa is achieved in pure nickel grains. This result suggests that compression is an effective method to suppress GB sliding and migration for achieving ultrahigh strength. This is also supported by the observation that the measured strength of coarse nickel in our compression test is higher than in conventional tension tests[2,18]. In real applications, materials could be under either tension or compression. Tension tests are common in traditional mechanical characterization. However, evaluation of strength by tensile loading is often technically difficult for nanograined metals especially for sub-10 nm grain sizes. Compressive strength measurements using radial DAC XRD enables studies of the mechanical properties of even sub-10 nm-sized metals. In this synchrotron-based study, deformation behavior and yield strength are obtained from the lattice changes of a large quantity of nano grains and exhibit reproducible trends in strength and grain size. Additionally, extrinsic factors like impurities and amorphous regions which are possibly introduced in conventional sample preparation methods could significantly affect the mechanical behaviors of nanograined metals. In our method, the strength is determined by the internal piezometer of crystalline lattice strain in pure nickel grains, which mitigate the effects of extrinsic factors.

Experimental work also indicates that partial dislocation-associated mechanisms improve the thermal stability of grain boundaries of nanograins[29]. If the grain boundaries of nanograined metals are sintered without grain coarsening, e.g. through severe plastic deformation or explosive shock annealing[30], large pieces of nanograined metals with ultrahigh strength can be potentially fabricated for mass applications. In summary, achieving an ultrahigh strength in pure nickel through grain refinement and grain boundary plasticity suppression provides a new strategy for designing ultra-strong and ultra-hard metals for future applications.

1 Schiøtz, J. & Jacobsen, K. W. A maximum in the strength of nanocrystalline copper. *Science* **301**, 1357-1359 (2003).

2 Schuh, C., Nieh, T. & Yamasaki, T. Hall–Petch breakdown manifested in abrasive wear resistance of nanocrystalline nickel. *Scripta Materialia* **46**, 735-740 (2002).

3 Knapp, J. & Follstaedt, D. Hall–Petch relationship in pulsed-laser deposited nickel films. *Journal of materials research* **19**, 218-227 (2004).

4 Meyers, M. A., Mishra, A. & Benson, D. J. Mechanical properties of nanocrystalline materials. *Progress in Materials Science* **51**, 427-556, doi:10.1016/j.pmatsci.2005.08.003 (2006).

5 Huang, X., Hansen, N. & Tsuji, N. Hardening by annealing and softening by deformation in nanostructured metals. *Science* **312**, 249-251 (2006).

6 Lu, L., Chen, X., Huang, X. & Lu, K. Revealing the maximum strength in nanotwinned copper. *Science* **323**, 607-610 (2009).

7 Koch, C. C. & Narayan, J. in *MRS Proceedings.* B5. 1.1 (Cambridge Univ Press).

8 Chen, B. *et al.* Texture of nanocrystalline nickel: probing the lower size limit of dislocation activity. *Science* **338**, 1448-1451, doi:10.1126/science.1228211 (2012).

9 Hughes, D. & Hansen, N. Exploring the limit of dislocation based plasticity in nanostructured metals. *Physical review letters* **112**, 135504 (2014).

10 Chen, M. *et al.* Deformation twinning in nanocrystalline aluminum. *Science* **300**, 1275-

1277, doi:10.1126/science.1083727 (2003).
11 Yamakov, V., Wolf, D., Phillpot, S. R., Mukherjee, A. K. & Gleiter, H. Dislocation processes in the deformation of nanocrystalline aluminium by molecular-dynamics simulation. *Nat Mater* **1**, 45-48, doi:10.1038/nmat700 (2002).
12 Shan, Z. *et al.* Grain boundary-mediated plasticity in nanocrystalline nickel. *Science* **305**, 654-657, doi:10.1126/science.1098741 (2004).
13 Zhou, X. *et al.* Reversal in the Size Dependence of Grain Rotation. *Physical Review Letters* **118**, 096101 (2017).
14 Chen, B., Zhu, L., Xin, Y. & Lei, J. Grain Rotation in Plastic Deformation. *Quantum Beam Science* **3**, 17 (2019).
15 Singh, A. K., Balasingh, C., Mao, H.-k., Hemley, R. J. & Shu, J. Analysis of lattice strains measured under nonhydrostatic pressure. *Journal of Applied Physics* **83**, 7567, doi:10.1063/1.367872 (1998).
16 Lutterotti, L., Vasin, R. & Wenk, H.-R. Rietveld texture analysis from synchrotron diffraction images. I. Calibration and basic analysis. *Powder Diffraction* **29**, 76-84 (2014).
17 Wang, H., Wu, P., Tomé, C. & Huang, Y. A finite strain elastic–viscoplastic self-consistent model for polycrystalline materials. *Journal of the Mechanics and Physics of Solids* **58**, 594-612 (2010).
18 Ebrahimi, F., Bourne, G., Kelly, M. S. & Matthews, T. Mechanical properties of nanocrystalline nickel produced by electrodeposition. *Nanostructured materials* **11**, 343-350 (1999).
19 Yamakov, V., Wolf, D., Phillpot, S., Mukherjee, A. & Gleiter, H. Deformation-mechanism map for nanocrystalline metals by molecular-dynamics simulation. *Nature materials* **3**, 43 (2004).

20 Van Swygenhoven, H., Derlet, P. & Frøseth, A. Stacking fault energies and slip in nanocrystalline metals. *Nature materials* **3**, 399-403 (2004).

21 Zhu, Y., Liao, X. & Wu, X. Deformation twinning in nanocrystalline materials. *Progress in Materials Science* **57**, 1-62 (2012).

22 Zepeda-Ruiz, L. A., Stukowski, A., Oppelstrup, T. & Bulatov, V. V. Probing the limits of metal plasticity with molecular dynamics simulations. *Nature* (2017).

23 Li, B., Li, B., Wang, Y., Sui, M. & Ma, E. Twinning mechanism via synchronized activation of partial dislocations in face-centered-cubic materials. *Scripta Materialia* **64**, 852-855 (2011).

24 Wang, J. & Huang, H. Shockley partial dislocations to twin: another formation mechanism and generic driving force. *Applied physics letters* **85**, 5983-5985 (2004).

25 Zhang, Z., Huang, S., Chen, L., Zhu, Z. & Guo, D. Formation mechanism of fivefold deformation twins in a face-centered cubic alloy. *Scientific Reports* **7**, 45405 (2017).

26 A.W.THOMPSON, A. Yielding in nickel as a function of grain or cell size. *Acta Metallurgica* **23** (1975).

27 Hughes, D. & Hansen, N. The microstructural origin of work hardening stages. *Acta Materialia* **148**, 374-383 (2018).

28 Hu, J., Shi, Y. N., Sauvage, X., Sha, G. & Lu, K. Grain boundary stability governs hardening and softening in extremely fine nanograined metals. *Science* **355**, 1292-1296, doi:10.1126/science.aal5166 (2017).

29 Huang, Q. *et al.* Nanotwinned diamond with unprecedented hardness and stability. *Nature* **510**, 250-253 (2014).

30 Zheng, S. *et al.* High-strength and thermally stable bulk nanolayered composites due to twin-induced interfaces. *Nature communications* **4**, 1696 (2013).

FIGURE LEGENDS:

Figure 1│Size strengthening of nanograined nickel. a, Azimuthally ($0\sim360^0$) unrolled diffraction images of nickel at different pressures. The black arrows indicate the axial compression direction. **b,** Differential stress vs lattice strain of nickel (see Supplementary Information). Note that for some of the data points the error bars are smaller than the sizes of symbols. **c,** Extrapolated yield strength of nickel at ambient conditions without GB sliding (from EVPSC simulations) vs grain size. The yield strength of nanograined (nc) Cu is obtained from MD simulations (Ref. 1) and experimental data of nanotwinned (nt) Cu [(Ref. 6)] and nanograined Ni (Ref. 2 and Ref. 18). The yield strength value of nickel in Ref. 2 is taken as 1/3 of its hardness. For nt-Cu, *d* represents the twin thickness. Inverse Hall-Petch effect has been reported for both Cu (Ref. 1 and Ref. 6) and Ni (Ref. 2). The smallest grain size of nickel in the study of Ref. 2 is 12 nm.

Figure 2│Inverse Pole Figures for the texture evolution of nickel with various grain sizes. Note that no starting texture exists in all raw samples. t and ε represent differential stress and lattice strain, respectively. Texture strength is expressed as multiples of random distribution (m.r.d.), where m.r.d. = 1 denotes a random distribution and a higher m.r.d. number represents a stronger texture.

Figure 3│Computational simulation results and the modified Hall-Petch relationship. a, Comparison of simulated grain size-dependent critical stresses for activating dislocations and grain boundary deformation in nanograined nickel at different pressures. "⊥" represents dislocation. **b,** Critical grain size d_c^2 as a function of pressure. **c,** The predicted yield strength compared with the experimental data for nanograined nickel. **d,** Classic MD simulation of 3-nm sized Ni compressed with 10% volume strain. Green color represents partial dislocations associated with stacking faults, twins and grain boundaries. Perfect dislocations are colored in blue. A small number of 1/3<001> (Hirth), 1/6 <110> (Stair-rod) and other types of dislocations can be identified (colored in yellow, purple and red).

Figure 4│TEM examinations of 3 nm (a), 20 nm (c) and 200 nm (d) nickel samples quenched from 40 GPa. (b) is a sketch showing the analysis of dislocations observed in the lower part of the middle grain in (a). Note the reactions of partial dislocations forming Lomer-Cottrell locks and a stair rod. "SF" represents the stacking faults. Stacking faults, twins, and few full dislocations can be found in 3 and 20 nm nickel samples. A high density of full dislocations is observed in the 200 nm nickel grains (inset of Fig. 4d).

Acknowledgements We thank Drs. Ke Lu, Dorte Juul Jensen, Niels Hansen, Shun-ichiro Karato, Guohua Fan, Jinling Liu and Feng Zhao for pre-review and discussions. X.Z. thanks Lin Feng for EVPSC tutoring. We acknowledge support from the National Natural Science Foundation of China (NSFC) under grant numbers U1530402 and 11811530001. X.Z. acknowledges the ALS Doctoral Fellowship in Residence Program and Collaborative Postdoctoral Fellowship Program. L.M. acknowledges support from CDAC and NSF EAR-1654687. Z.Q.F., T.L.H., and X.H. acknowledge the support from the State Key Research & Development Program of MOST of China (2016YFB0700400). This research used resources of the Advanced Light Source, which is a DOE Office of Science User Facility under contract no. DE-AC02-05CH11231, and Shanghai Synchrotron Radiation Facility (SSRF).

Author contributions B.C. conceived the project. X.H. directed the TEM examinations. J.X., H.D., H.Z. and K.L. contributed to nanocrystal synthesis. X.Z., B.C., L.M., J.Y., N.T. and M.K. contributed to high-pressure XRD experiments. Z.Q.F., Y.J.W., D.A.H., T.L.H. and X.H. contributed to TEM experiments and analysis. L.Z., H.S., Q.L. and Y.M. contributed to computational and molecular dynamics simulations. X.Z. and L.M. contributed to EVPSC modeling. X.Z. and B.C. wrote the manuscript. All authors discussed the results and commented on the manuscript.

Competing interests The authors declare no competing interests.

Additional information

Correspondence and requests for materials should be addressed to B.C. (chenbin@hpstar.ac.cn) and X.H.(xiaoxuhuang@cqu.edu.cn).

Data availability

The data that support the findings of this study are available from the corresponding authors upon reasonable request.

Extended Data Figure Legends:

Extended Data Fig. 1 | The experimental setup of radial DAC XRD.

Extended Data Fig. 2 | Grain size distribution of nickel samples. a, b, c, d, Grain size distribution of 3 nm nickel (Image courtesy of nanoComposix), 8 nm, 12 nm nickel and 20 nm nickel (Image courtesy of Nanomaterialstore); **e, f, g, h**, Grain size distribution of 40, 70, 100 and 200 nm nickel. The particle sizes of the nickel samples were re-checked with XRD characterization.

Extended Data Fig. 3 | TEM and SEM characterization of raw 3 nm (a), 8 nm (b), 12 nm (c), 20 nm (d), 40 nm (e), 70 nm (f), 100 nm (g) and 200 nm (h) nickel samples before compression.

Extended Data Fig. 4 | Plot of differential stress vs hydrostatic lattice strain in the nickel of various grain sizes. The circles, squares and triangles represent (220), (200) and (111) lattice planes, respectively. Strong strength anisotropy is exhibited for different lattice planes, especially in smaller grain size. The lattice strain is calculated from the change in the unit cell parameter at a given applied stress and the ambient pressure unit cell parameter. The error bar of differential stress is calculated based on the error of *Qhkl* and Eqs. (6-9). Note that for some of the data points the error bars are smaller than the sizes of symbols.

Extended Data Fig. 5 | EVPSC modeling results of nickel. a, Comparison between simulated *Q(hkl)* curves vs pressure and measured *Q(hkl)* values obtained from experiments; b, simulated texture of nickel at the highest strain (pressure); c, Simulated differential stress of nickel vs plastic strain during zero pressure compression; d, Extrapolated yield strength of nickel at ambient conditions without GB sliding. The size strengthening trend is consistent with that shown in Figs. 1b, although the strength of 40 nm nickel obtained with EVPSC is slightly lower.

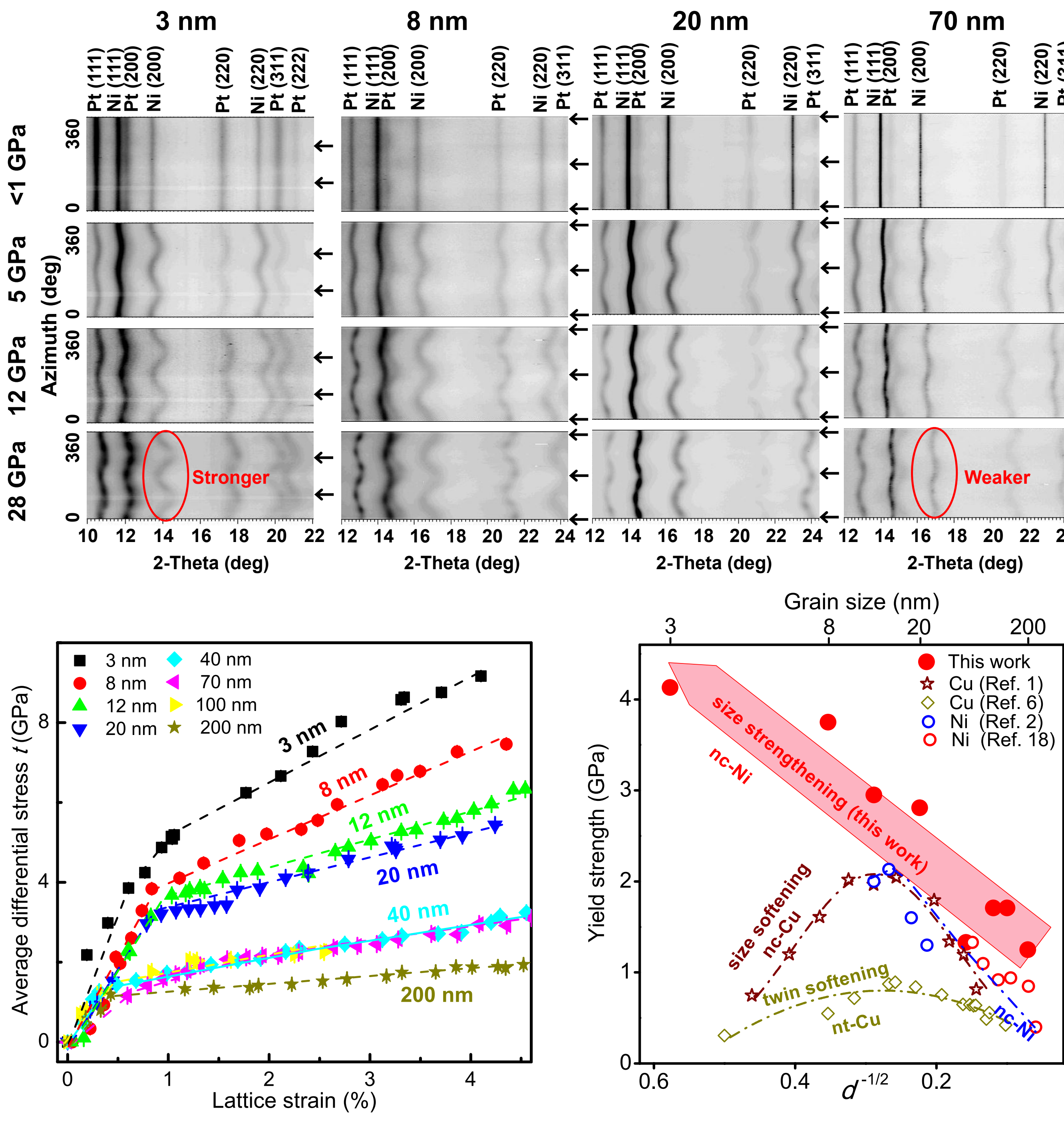

3 nm
8 nm
20 nm
70 nm
Pt (111)
Ni (111)
Pt (200)
Ni (200)
Pt (220)
Ni (220)
Pt (311)
Pt (222)
<1 GPa
5 GPa
12 GPa
28 GPa
Azimuth (deg)
Stronger
Weaker
2-Theta (deg)
Average differential stress t (GPa)
Lattice strain (%)
3 nm
8 nm
12 nm
20 nm
40 nm
70 nm
100 nm
200 nm
Grain size (nm)
Yield strength (GPa)
$d^{-1/2}$
This work
Cu (Ref. 1)
Cu (Ref. 6)
Ni (Ref. 2)
Ni (Ref. 18)
size strengthening (this work)
nc-Ni
size softening
nc-Cu
twin softening
nt-Cu

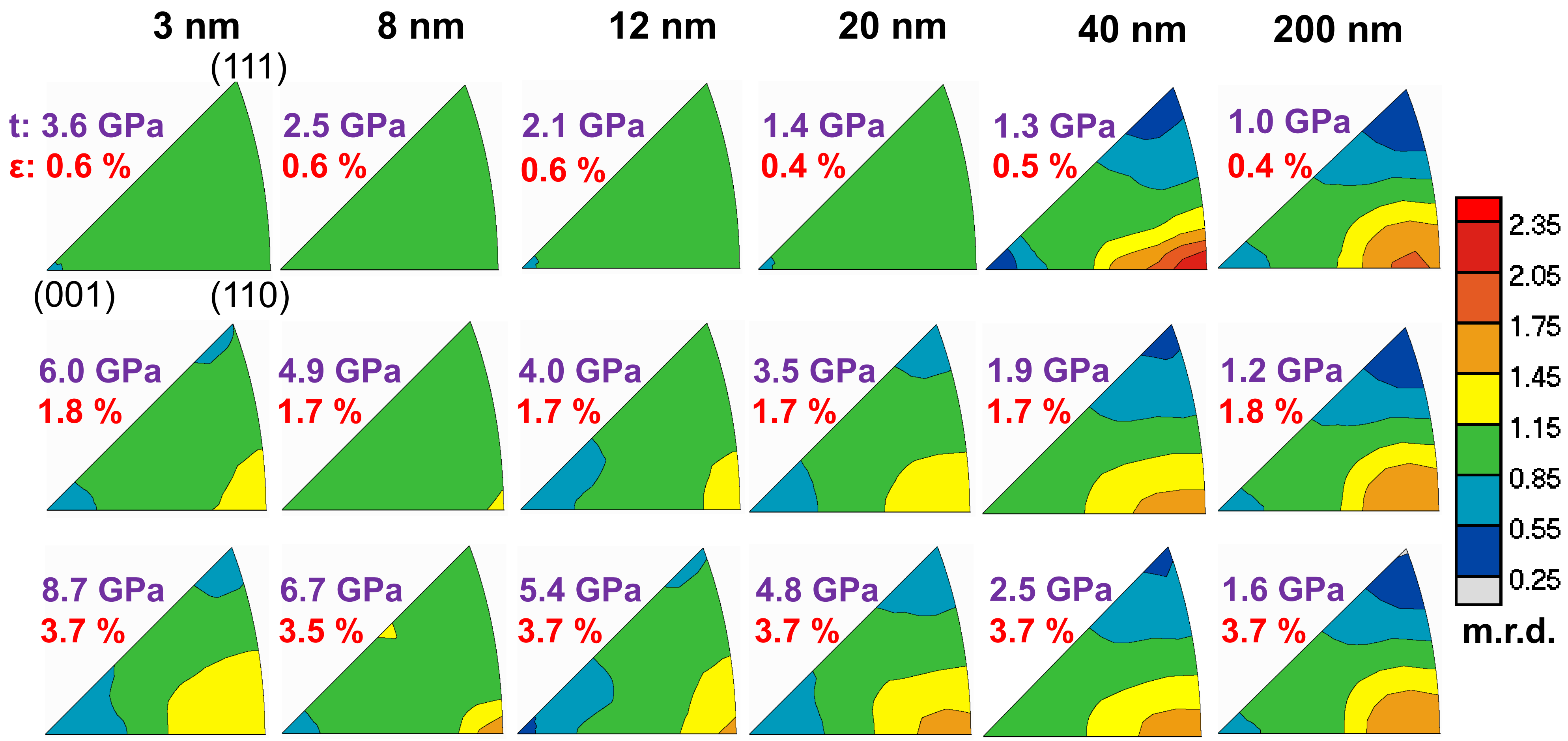
3 nm
8 nm
12 nm
20 nm
40 nm
200 nm
(111)
(001)
(110)
t: 3.6 GPa
ε: 0.6 %
2.5 GPa
0.6 %
2.1 GPa
0.6 %
1.4 GPa
0.4 %
1.3 GPa
0.5 %
1.0 GPa
0.4 %
6.0 GPa
1.8 %
4.9 GPa
1.7 %
4.0 GPa
1.7 %
3.5 GPa
1.7 %
1.9 GPa
1.7 %
1.2 GPa
1.8 %
8.7 GPa
3.7 %
6.7 GPa
3.5 %
5.4 GPa
3.7 %
4.8 GPa
3.7 %
2.5 GPa
3.7 %
1.6 GPa
3.7 %
2.35
2.05
1.75
1.45
1.15
0.85
0.55
0.25
m.r.d.

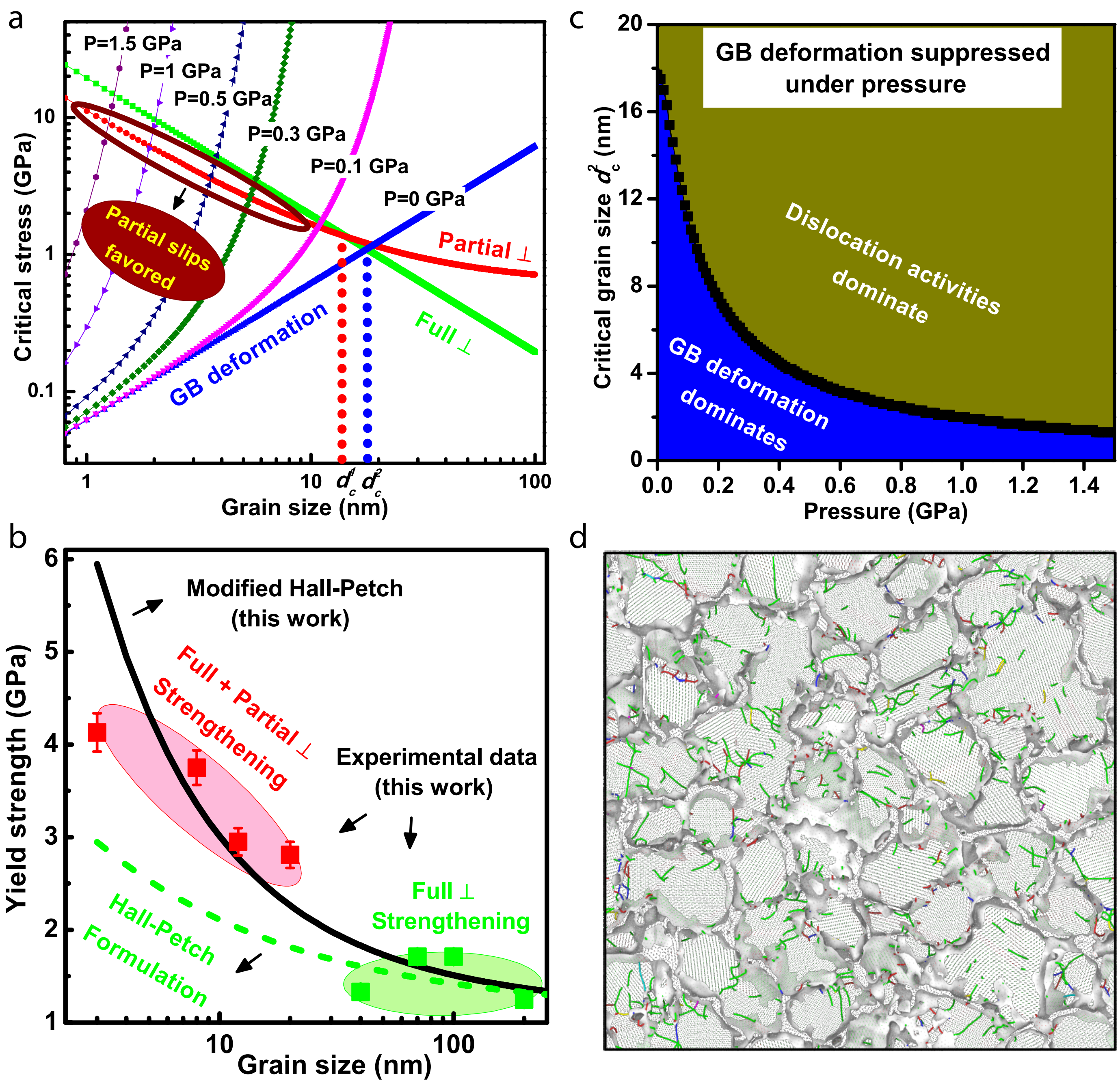

a
P=1.5 GPa
P=1 GPa
P=0.5 GPa
P=0.3 GPa
P=0.1 GPa
P=0 GPa
Partial slips favored
Partial ⊥
Full ⊥
GB deformation
Critical stress (GPa)
Grain size (nm)
d_c^1 d_c^2
b
Modified Hall-Petch (this work)
Full + Partial ⊥ Strengthening
Experimental data (this work)
Full ⊥ Strengthening
Hall-Petch Formulation
Yield strength (GPa)
Grain size (nm)
c
GB deformation suppressed under pressure
Dislocation activities dominate
GB deformation dominates
Critical grain size d_c^2 (nm)
Pressure (GPa)
d

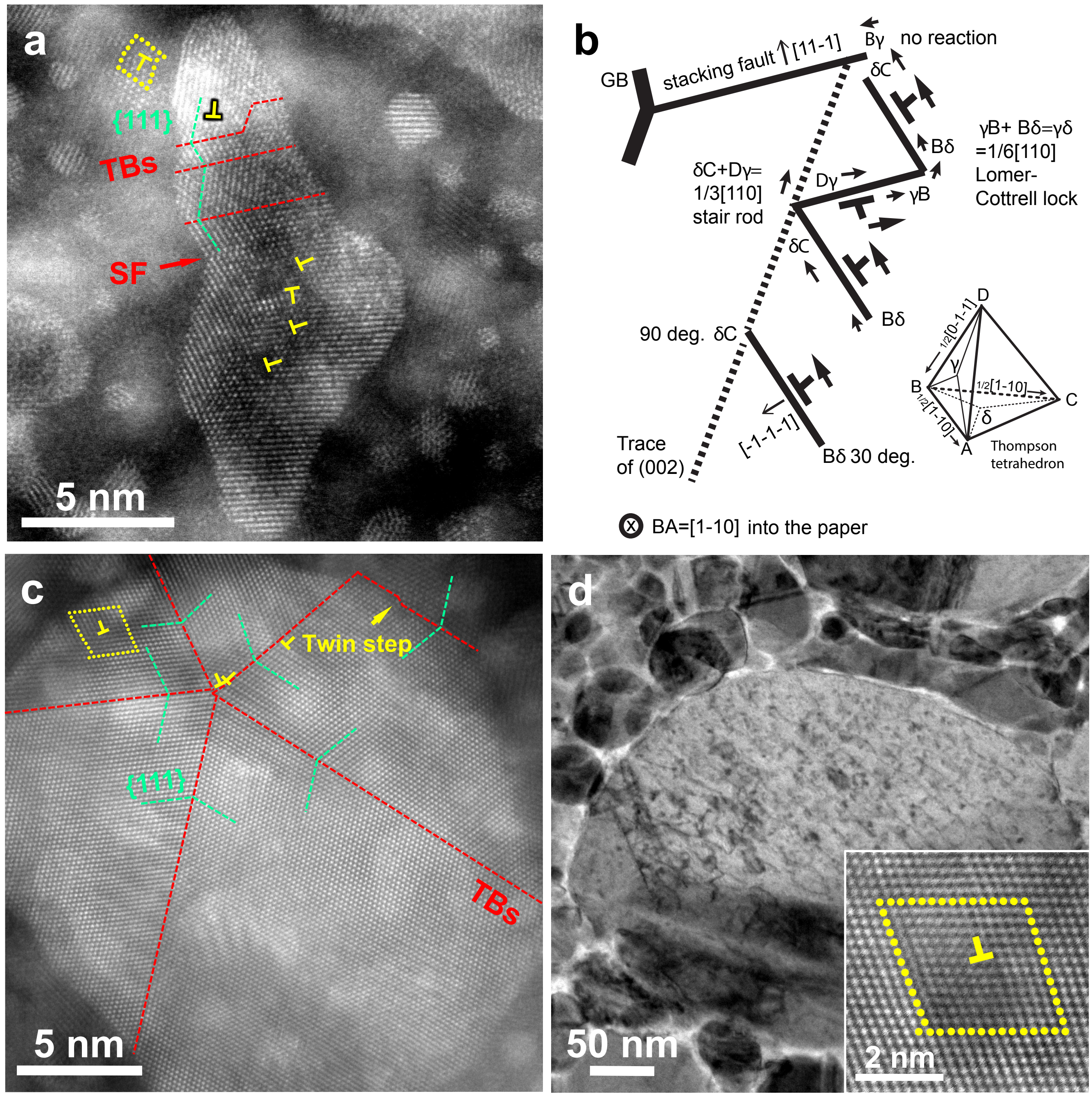
a
{111}
TBs
SF
5 nm
b
stacking fault
[11-1]
GB
Bγ
no reaction
δC
Bδ
γB+ Bδ=γδ
=1/6[110]
Lomer-
Cottrell lock
δC+Dγ=
1/3[110]
stair rod
Dγ
γB
δC
Bδ
90 deg. δC
[-1-1-1]
Bδ 30 deg.
Trace
of (002)
D
1/2[0-1-1]
B
1/2[1-10]
C
1/2[1-10]
A
Thompson
tetrahedron
BA=[1-10] into the paper
c
Twin step
{111}
TBs
5 nm
d
50 nm
2 nm